The extension of the Multiple Sphere T Matrix code to include multiple plane boundaries and 2-D periodic systems

D. W. Mackowski[a]

[a]Department of Mechanical Engineering, Auburn University, Auburn, AL 36849, U.S.A.

Abstract

An extension of the parameter space available to the Multiple Sphere T Matrix (MSTM) code is described. The code can now calculate electromagnetic scattering and absorption characteristics of multiple spheres that are placed adjacent to multiple plane boundaries perpendicular to the z direction, with each boundary separating layers of different complex refractive index. The spheres can also form infinitely periodic structures in the $x - y$ plane. The code retains all previous features, such as the spheres being comprised of optically active materials and having positions internal or external to other spheres. Example calculations to demonstrate the veracity of the code.

1. Introduction

Ten years ago Michael Mishchenko and I made available a fortran–90 code for calculating the electromagnetic scattering properties of multiple sphere systems [1]. The code implemented the exact, superposition–based solution to the frequency–domain Maxwell's equations for multiple homogeneous spheres, and could provide cross sections and angular–dependent scattering matrix values for either fixed orientations of the cluster relative to the incident plane wave, or, via analytical T matrix procedures, random orientations. Over the years the code has gone through several additions and modifications, such as the incorporation of optically active media within the spheres and the generalization of the sphere positions so that they could reside internally to other spheres [2].

The purpose of this paper is to announce yet another new set of bells and whistles for the code. Specifically, the code can now incorporate multiple parallel plane boundaries that separate regions (or layers) of different refractive indices, with the spheres being allowed to reside in any and/or all of the separate regions. The system of spheres, distributed among the plane boundaries, can represent a single cluster, or it can be analytically repeated with period W_x, W_y in the lateral plane to $\pm\infty$ to form a 2–D periodic structure.

None of the additions represent a novel extension to the multiple sphere superposition problem. Stefanou and Modinos developed a formulation for the periodic sphere–on–a–substrate problem in 1991 [3], and a multipole–based, multiple sphere formulation of

the 2D periodic model has been recently presented in [4]. The 2–D periodic scattering problem, in particular, has been receiving substantial attention due to the relevance to photonic arrays and metasurfaces [5, 6, 7].

The overall form of the superposition solution is not radically changed by the introduction of plane boundaries or 2-D periodic conditions: each sphere has an associated scattered field multipole expansion, the scattered field from one sphere produces an exciting field at another field that is described by a multipole Green's function, and the application of continuity relations at each sphere surface result in a system of linear equations for the scattered field expansion coefficients. The new features, however, do present significant computational complications in regard to accurately and precisely calculating the multipole Green's function over a wide range of length scales (relative to the wavelengths) and refractive indices that characterize the system; these issues will be presented in the course of the paper.

Computational results from the code have been successfully tested against results found in the literature [3, 6]. The electric and magnetic complex vector amplitudes calculated by the code have also been shown to correctly meet boundary continuity and symmetry requirements for a wide range of plane boundary and 2–D periodic conditions. That said, it is certain that unidentified parameter spaces exist where the code will fail to give the true solution. With luck, such spaces will be clearly obvious in that the code will produce obviously unphysical results and/or NANs. The code also has alarms in place that will ring when convergence or error criteria are not met, and the user is admonished to pay attention to such signals.

2. Formulation

2.1. Basic superposition concepts

In what follows all quantities are implicitly dimensionless. Lengths are scaled using the free space wavenumber $k_0 = 2\pi/\lambda_0$, with λ_0 denoting the free space wavelength of the exciting incident wave, electric field amplitude is relative to the amplitude of the exciting wave, and refractive indices are relative to $\sqrt{\epsilon_0}$, where ϵ_0 is the permittivity of free space. A time harmonic factor of $\exp(-i\omega t)$ is adopted. The system is taken to consist of N_B parallel plane boundaries with surface normals in the z direction. The first boundary is fixed at $z = Z_1 = 0$, and the remainder located at $z = Z_2, Z_3, \ldots Z_{N_B}$, with all $Z_B \geq 0$. The media below $z = 0$ is denoted as layer $\ell = 0$, that between $z = 0$ and Z_2 as layer $\ell = 1$, and so on. Layers 0 and N_B are half spaces extending to - and $+ \infty$. The material within each layer is isotropic and characterized by a complex refractive index $m_\ell, \ell = 0, 1 \ldots N_B$.

Distributed within the layers are a group (or unit cell) of N_S spherical particles, each characterized by a position vector $\mathbf{r}^i$ and a radius a^i. Each sphere is embedded within a single layer – they do not overlap with each other nor do they cross a plane boundary – yet aside from this constraint they can be anywhere. The code allows the spherical particles to contain other spheres and/or optically active material. Such details, however, are not especially germane to the plane boundary and periodic lattice formulations. To simplify the presentation, the N_S spheres will be taken to be homogeneous and isotropic. The unit cell of N_S spheres may be repeated in the x, y plane to $\pm\infty$, with period W_x, W_y; for such conditions it is implied that the unit cell of spheres can be repeated periodically without sphere overlap occurring at the cell boundaries.

Per the usual scattering ansatz, the exciting field is the field that would exist in the plane boundary system when all scattering particles are absent. It will take the general form, within each layer, of a superposition of upwards and downwards-directed plane waves which result from a plane wave source at some defined (real or imaginary) boundary. The typical situation has the source boundary located in the far-field of layer 0 or N_B and producing a unit-amplitude wave propagating towards the system with a set incidence direction. Other situations can also be examined under the formulation, such as the excitation of slab waveguide modes by an evanescent source along the first boundary.

The scattered field is the difference in the fields with and without the particles present, and can be described mathematically as a superposition of individual scattered fields associated with each sphere. The mathematical details of this superposition will depend on the specific location of the evaluation point relative to the spheres and the plane boundaries, and whether the system is finite or 2D periodic. Such details will be developed subsequently. For all situations, the scattered field associated with sphere i, and the exciting field, can be approximated on the exterior surface of i by truncated vector spherical wave function (VSWF) expansions of the outgoing and regular types. The coefficients in the expansions, denoted by $a_{\mathbf{n}}^i$ and $f_{\mathbf{n}}^i$, will satisfy a set of linear equations of the form

$$a_{\mathbf{n}}^i = \overline{a}_{\mathbf{n}}^i \left(f_{\mathbf{n}}^i + \sum_{j=1}^{N_S} \sum_{\mathbf{l}}^{M_S^j} G_{\mathbf{nl}}(\mathbf{r}^i, \mathbf{r}^j) a_{\mathbf{l}}^j \right) \tag{1}$$

In the above and what follows, boldface subscripts $\mathbf{n}$, $\mathbf{l}$ denote length-3 index vectors containing VSWF degree, azimuth order, and mode (TM or TE), i.e., $\mathbf{n} = (n_2, n_1, n_3)$ with $n_1 = 1, 2 \ldots L_S^i, n_2 = -n_1, -n_1 + 1, \ldots n_1,\ n_3 = 1, 2$; L_S^i is the truncation degree associated with sphere i and will typically scale with $|a^i \mathsf{m}_{\ell(i)}|$, where $\ell(i)$ denotes the layer containing sphere i. The indices are ordered $\mathbf{n} = n_2, n_1, n_3$ as opposed to the obvious, sequential manner simply to be consistent with previous publications. The total number of $a_{\mathbf{n}}^i$ coefficients for sphere i is $M_S^i = 2L_S^i(L_S^i + 2)$, and the sum over vector index $\mathbf{l}$ implies sum over all M_S^j values of the indices. The quantity $\overline{a}_{\mathbf{n}}^i$ is the Lorenz-Mie coefficient for the sphere, which is dependent on the sphere radius and internal/external refractive indices (and independent of VSWF azimuth order, i.e., $\overline{a}_{\mathbf{n}}^i = \mathbf{a}_{(n_1, n_3)}^i$). The matrix $G_{\mathbf{nl}}(\mathbf{r}^i, \mathbf{r}^j)$ is the multipole Green's function (MGF) for the system; this gives the $\mathbf{n}$ element of the regular VSWF field, centered about $\mathbf{r}^i$, resulting from the $\mathbf{l}$ element of an outgoing VSWF source at $\mathbf{r}^j$. The MGF will depend explicitly on the plane boundary and periodic configurations of the system.

The total number of equations in Eq. (1) is $M_{eqns} = \sum M_S^i$. Calculation of the full polarimetric scattering properties of the system, for a given excitation state, requires solution of Eq. (1) for two mutually orthogonal polarization states of the exciting field.

3

2.2. Finite systems

2.2.1. Fundamental integral relations

Derivation of $G_{\mathbf{nl}}(\mathbf{r}^i, \mathbf{r}^j)$ in Eq. (1) makes use of the integral expression for the outgoing VSWF evaluated in a medium with refractive index m[8, 9, 10]:

$$\mathbf{N}_{\mathbf{l}}^{(3)}(\mathsf{m}, \mathbf{r} - \mathbf{r}^j) = -\frac{1}{\sqrt{2\pi}} \sum_{p=1}^{2} \int_{-\infty}^{\infty} \int_{-\infty}^{\infty} \Pi_{\mathbf{l},p}(\sigma \mathsf{k}_z, \alpha) \, \mathbf{h}_p(\mathbf{k}_\rho, \mathsf{m}) \, e^{i\mathsf{m}(\mathbf{r} - \mathbf{r}^j) \cdot \mathbf{k}} \, \frac{d\mathsf{k}_x d\mathsf{k}_y}{\mathsf{m}^2 \mathsf{k}_z} \quad (2)$$

with

$$\mathbf{k} = \frac{1}{\mathsf{m}} \mathbf{k}_\rho + \sigma \hat{\mathbf{z}} \mathsf{k}_z = \frac{\mathsf{k}_\rho}{\mathsf{m}} (\hat{\mathbf{x}} \cos\alpha + \hat{\mathbf{y}} \sin\alpha) + \sigma \hat{\mathbf{z}} \mathsf{k}_z = \frac{1}{\mathsf{m}} (\hat{\mathbf{x}} \mathsf{k}_x + \hat{\mathbf{y}} \mathsf{k}_y) + \sigma \hat{\mathbf{z}} \mathsf{k}_z \quad (3)$$

$$\mathsf{k}_z = \frac{1}{\mathsf{m}} \left(\mathsf{m}^2 - \mathsf{k}_\rho^2 \right)^{1/2} \quad (4)$$

$$\alpha = \tan^{-1} \left(\frac{\mathsf{k}_y}{\mathsf{k}_x} \right), \quad \sigma = \operatorname{sign} z - z^j \quad (5)$$

$$\mathbf{h}_1 = \mathsf{k}_z (\hat{\mathbf{x}} \cos\alpha + \hat{\mathbf{y}} \sin\alpha) - \sigma \hat{\mathbf{z}} \frac{\mathsf{k}_\rho}{\mathsf{m}}, \quad \mathbf{h}_2 = -\hat{\mathbf{x}} \sin\alpha + \hat{\mathbf{y}} \cos\alpha \quad (6)$$

The quantity $\Pi_{\mathbf{l},p}$ is the pth component of the vector spherical harmonic (VSH) function $\mathbf{\Pi}_{\mathbf{l}}$, with $p = 1, 2$ denoting polar (a.k.a., parallel) and azimuthal (perpendicular) directions. Using the expanded index notation $\mathbf{l} = klq$, the VSH is defined by

$$\mathbf{\Pi}_{kl\,1}(\mathsf{k}_z, \alpha) = \frac{r}{\sqrt{l(l+1)}} \nabla Y_{kl}(\mathsf{k}_z, \alpha) \quad (7)$$

$$\mathbf{\Pi}_{kl\,2}(\mathsf{k}_z, \alpha) = \frac{1}{\sqrt{l(l+1)}} \mathbf{r} \times \nabla Y_{kl}(\mathsf{k}_z, \alpha) \quad (8)$$

with $Y_{kl}(\mathsf{k}_z, \alpha)$ denoting the spherical harmonic:

$$Y_{kl}(\mathsf{k}_z, \alpha) = \left(\frac{(2l+1)(l-k)!}{4\pi(l+k)!} \right)^{1/2} P_l^k(\mathsf{k}_z) e^{ik\alpha} \quad (9)$$

The quantities k_ρ and k_z are referred to as the lateral and normal wavenumbers. Note that $\mathbf{h}_p \exp(i\mathsf{m}(\mathbf{r} - \mathbf{r}^j) \cdot \mathbf{k})$ describes a $p-$polarized plane wave with wavevector $\mathbf{k}$, in that $\mathbf{k}, \mathbf{h}_1$, and $\mathbf{h}_2$ are mutually orthogonal. For real m, this wave is propagating and evanescent for $\mathsf{k}_\rho <$ and $> \mathsf{m}$, respectively. Convergence of the integral requires $|z - z^j| > 0$.

Equation (2) shows that the outgoing VSWF is equivalent to a 2D Fourier transform, in the lateral plane, of vector plane waves dotted with the VSH function. The plane waves emerge from a source at $z = z^j$, and are directed upwards or downwards depending on the sign of $z - z^j$. This source field, in a plane boundary system, will produce a secondary plane wave field due to reflection and transmission at the boundaries, the description of which can be obtained by a generalized Fresnel analysis of the system. The MGF is obtained by expanding this secondary field in regular VSWFs centered about some secondary origin $\mathbf{r}^i$. For homogeneous media, in which the Fresnel relations are independent of azimuth angle α, the 2D integral can be transformed to cylindrical coordinates

4

and analytically integrated over azimuth angle α, resulting in a Hankel transform-type formula. The end result is

$$G_{\mathbf{n}\mathbf{l}}(\mathbf{r}^i, \mathbf{r}^j) = 4\pi \mathrm{i}^{|l_2 - n_2|} e^{\mathrm{i}(l_2 - n_2)\phi^{i-j}} \int_0^\infty J_{|l_2 - n_2|}(\mathrm{k}_\rho \, \rho^{i-j})$$

$$\times \sum_{\sigma = \pm 1} \sum_{\sigma' = \pm 1} \sum_{p=1}^2 \left(\Pi_{\mathbf{n},p}^\dagger(\sigma \, \mathrm{k}_{z,i}, 0) G_p^{\sigma\sigma'}(\mathrm{k}_\rho, z^i, z^j) \Pi_{\mathbf{l},p}(\sigma' \, \mathrm{k}_{z,j}, 0) \right) \frac{\mathrm{k}_\rho \, d\mathrm{k}_\rho}{\mathsf{m}_{\ell(j)}^2 \mathrm{k}_{z,j}} \quad (10)$$

In the above, ϕ^{i-j} and ρ^{i-j} are the angle and distance, in the $x - y$ plane, of target i relative to source j, $J_m(x)$ is the ordinary Bessel function of order m, $\Pi_{\mathbf{n},p}^\dagger$ denotes the conjugated function $\Pi_{\mathbf{n},p}$ (i.e., the conjugate does not apply to the argument, for cases where k_z is complex), and n_2, l_2 denote the azimuth order part of the indices $\mathbf{n}$, $\mathbf{l}$. The normal wavenumbers $\mathrm{k}_{z,j}$ and $\mathrm{k}_{z,i}$ are evaluated from Eq. (4) using the refractive indices corresponding to the layers containing origins j and i.

2.2.2. Plane Boundary Green's Function

The plane boundary Green's function (PBGF) in Eq. (10), denoted as $G_p^{\sigma\sigma'}(\mathrm{k}_\rho, z^i, z^j)$, gives the amplitude of a σ–directed (=1,up, or -1, down), p-polarized wave at the target position z^i due to unit-amplitude σ'–directed source wave emitted at the source location z^j. It can be decomposed into indirect and direct parts:

$$G_p^{\sigma\sigma'}(\mathrm{k}_\rho, z, z') = \widetilde{G}_p^{\sigma\sigma'}(\mathrm{k}_\rho, z, z') + \delta_{\sigma - \sigma'} \delta_{\ell - \ell'} \delta_{\mathrm{sign}(z - z') - \sigma} e^{\mathrm{i}\sigma \mathsf{m}_r \mathrm{k}_{z,r}(z - z')} \quad (11)$$

where ℓ, ℓ' denote the layers containing z, z', and $\delta_n = 0, 1$ for $n \neq, = 0$ is the Kronecker delta function. The indirect PBGF, $\widetilde{G}$, accounts for the effects of the plane boundaries and is zero when such boundaries are absent. This part will always result in a convergent integral in Eq. (10) (providing z^i or z^j are removed from a plane boundary). The direct part in Eq. (11) (the second part) results, when replaced into Eq. (10) and analytically integrated, in the traditional outgoing VSWF translation matrix $H_{\mathbf{n}\mathbf{l}}(\mathbf{r}, \mathbf{r}')$, a.k.a., the free-space MGF. Accordingly, the MGF can be split into boundary and free-space parts, via

$$G_{\mathbf{n}\mathbf{l}}(\mathbf{r}, \mathbf{r}') = \widetilde{G}_{\mathbf{n}\mathbf{l}}(\mathbf{r}, \mathbf{r}') + \delta_{\ell - \ell'} \left(1 - \delta_{|\mathbf{r} - \mathbf{r}'|} \right) H_{\mathbf{n}\mathbf{l}}(\mathbf{r}, \mathbf{r}') \quad (12)$$

The $(1 - \delta_{|\mathbf{r} - \mathbf{r}'|})$ term in the above serves to zero the free space part for the specific case of sphere self–interaction, i.e., $j = i$ in Eq. (1).

The PBGF is obtained via solution of a linear set of equations that apply the continuity equations at each plane boundary. To develop such equations, consider the case where a source of plane waves exists at z_s, within layer s, and emits in the σ_s direction with lateral wavenumber k_ρ. Denote as $F_{out,p}^{\sigma,n}(\mathrm{k}_\rho)$ the complex amplitude of the p-polarized plane wave leaving boundary n in the σ direction. For $\sigma = 1$ this wave is directed into layer n (above the boundary), and for $\sigma = -1$ into layer $n - 1$ (below the boundary). At each boundary a T matrix relationship can be applied, so that

$$F_{out,p}^{\sigma,n}(\mathrm{k}_\rho) = \sum_{\sigma' = \pm 1} T_p^{\sigma\sigma' n}(\mathrm{k}_\rho) F_{in,p}^{\sigma',n}(\mathrm{k}_\rho) \quad (13)$$

in which $F_{in,p}^{\sigma',n}(\mathrm{k}_\rho)$ is the complex amplitude of the p-polarized wave arriving at boundary n in the σ' direction, and $T_p^{\sigma\sigma' n}$ are the Fresnel coefficients for the boundary (given in the Appendix).

5

The incoming amplitude at one boundary can be related to the outgoing amplitudes at adjacent boundaries via a simple application of complex phase rules for plane waves:

$$F_{in,p}^{1,n}(\mathrm{k}_\rho) = e^{i\,\mathrm{k}_{z,n-1}(Z_n - Z_{n-1})} F_{out,p}^{1,n-1}(\mathrm{k}_\rho) + e^{i\,\mathrm{k}_{z,n-1}(Z_n - z_s)} \delta_{\sigma_s - 1} \delta_{n-1-s} \tag{14}$$

$$F_{in,p}^{-1,n}(\mathrm{k}_\rho) = e^{i\,\mathrm{k}_{z,n}(Z_{n+1} - Z_n)} F_{out,p}^{-1,n+1}(\mathrm{k}_\rho) + e^{i\,\mathrm{k}_{z,n}(z_s - Z_n)} \delta_{\sigma_s + 1} \delta_{n-s} \tag{15}$$

The terms containing the delta functions account for the contribution of the source. Furthermore, $F_{out,p}^{1,n} = 0$ for $n = 0$, $F_{out,p}^{-1,n} = 0$ for $n = N_B + 1$, since there are no real boundaries below boundary 1 nor above boundary N_B. Replacing Eqs. (14) and (15) into Eq. (13) results in a $2 \times N_B$ set of linear equations for $F_{out,p}^{\sigma,n}(\mathrm{k}_\rho)$ for each lateral wavenumber k_ρ, polarization p and source direction σ_s. The indirect PBGF corresponds to the outgoing amplitude at the target point z_t, located in layer t; this will be given by

$$\widetilde{G}_p^{1\sigma_s}(\mathrm{k}_\rho, z_t, z_s) = e^{i\,\mathrm{k}_{z,t}(z_t - Z_n)} F_{out,p}^{1,t} \tag{16}$$

$$\widetilde{G}_p^{-1\sigma_s}(\mathrm{k}_\rho, z_t, z_s) = e^{i\,\mathrm{k}_{z,t}(Z_{n+1} - z_t)} F_{out,p}^{-1,t+1} \tag{17}$$

2.2.3. Numerical Issues

For the case of a single boundary separating two half-spaces a simple formula, involving the boundary Fresnel coefficients and the phase lags for the source and target to the boundary, emerges for the PBGF. It is not difficult to analytically solve the equations for a pair of boundaries representing a finite-thickness layer bordered by the two half spaces. The computational approach used in the code avoids such algebraic complications, and solves the set of equations for $F_{out,p}^{\sigma,n}$ numerically for each given source and target polarization and direction. Two numerical methods are used: the first recognizes that the system of equations can be put into a block-tridiagonal matrix form, for which a recursive algorithm can be applied to calculate the Green's function in order–N_B steps. This method, however, becomes unstable when the real parts of the exponents appearing in Eqs. (14) and (15) become large. For such conditions a second method using simple iteration, akin to an order-of-scattering expansion of the equations, is applied.

Evaluation of the integral in Eqs. (10) must be done numerically. As the integrand will exhibit (often highly) oscillatory behavior as a result of the Green's and Bessel functions, as well as singularities from the $1/\mathrm{k}_{z,\mathrm{m}_i}$ term as well as possible poles in the Green's function lying on or near the integration path, a relatively large body of work has been performed to develop accurate and efficient methods as applied to Sommerfeld integrals. Image methods express the Green's function as a Laplace transform in the z coordinate, and lead to a formula in which $\widetilde{G}_{\mathbf{nl}}(\mathbf{r}^i, \mathbf{r}^j)$ appears as a superposition of outgoing translation matrices evaluated between $\mathbf{r}^i$ and complex points along the z axis [11]. This approach, however, only appears valid when i and j are both in the same layer. Steepest descent methods make use of the symmetry of the Bessel function for positive and negative argument, allowing it to be replaced with the ordinary Hankel function and shifting the integration path from $\mathrm{k}_\rho : 0 \to \infty$ to $-\infty \to \infty$. By use of contour integration principles, this integration path can then be transformed in the complex plane so that it passes through the saddle point (i.e., the stationary phase point) in such a way to minimize the overall oscillation of the integration [12]. The reduced complexity of the integrand, however, can be more than offset by the ancillary issues of knowing, and dealing with, the branch cuts for the $N_B + 1$ square root functions (making

up k_{z,m_ℓ}) as well as the location of the poles in the Green's function, how the integration path passes relative to the poles, and calculating the residues if needed.

The approach taken here is to prioritize simplicity and generality over computational effort, in that numerical integration is performed on Eq. (10) almost as it appears. The one modification is based on the modified integration path by Cui and Chew [13], which involves shifting k into the complex plane slightly below the positive real axis, corresponding to $\mathrm{Im}\,(k_\rho) \sim 0.005$, to provide a degree of dampening in the integrand oscillations. The integration domain is broken into segments and a Gauss–Kronod quadrature method is applied to each segment. The GK method provides a means of estimating the error of the quadrature from a fixed set of quadrature points. If the error is above a set tolerance the segment is subdivided into two equal parts and the GK method is applied to each subdivided segment, with the algorithm performed recursively until the error criterion is met or until a maximum number of subdivisions has been reached. The integration is performed on a segment-to-segment basis along the $\mathrm{Re}\,(k_\rho)$ axis, until the relative contribution from the segment to the integral has dropped below a set tolerance.

2.2.4. Plane wave excitation model

The exciting field can take the form of a plane wave or a Gaussian beam. The plane wave is modeled as being emitted from a real or imaginary plane boundary located at $z = Z_{exi}$, directed in the $\sigma_{exi} = \pm 1$ direction, and characterized by a lateral wavenumber $k_{\rho,exi}$, azimuth ϕ_{exi}, and polarization $p_{exi} = 1, 2$. The complex amplitude of the p–polarized component, at some point $\mathbf{r}$ in the PB system, would be

$$E_{exi,p}(\mathbf{r}) = e^{ik_{\rho,exi}\rho\cos(\phi_{exi}-\phi)} \sum_{\sigma=\pm 1} G_p^{\sigma\sigma_{exi}}(k_{\rho,exi}, z, Z_{exi})E_{exi,p,0} \qquad (18)$$

where p denotes the polarization state of the incident wave, ρ and ϕ are the distance and angle of $\mathbf{r}$ in the lateral plane, relative to the common origin, and $E_{exi,p,0}$ is the source amplitude.

In the typical, external-excitation application, the source boundary Z_{exi} is in layer 0 at a position Z_{-B} that is below the minimum particle z position, the direction is $+1$, the amplitude $E_{exi,p,0} = 1$ for either $p = 1$ or 2, and the exciting lateral wavenumber obeys $k_{\rho,exi}/m_0 = \sin\theta_{inc} < 1$ where θ_{inc} is the angle of incidence in layer 0; this implicitly assumes layer 0 is lossless.

Equation (18) can also be used to model an exciting field corresponding to a slab waveguide mode. This field consists of a trapped plane wave contained, within one (or more) lossless dielectric layers, by total internal reflection. The net EM power transfer of the exciting field, in this case, is entirely in the lateral direction – no power (in the ideal, pure lossless dielectric limit) escapes to the bordering halfspaces. For a given plane boundary configuration, the waveguide (or resonant) modes occur at $k_\rho = k_s$, $s = s_1, s_2 \ldots$ values for which system Green's function is singular; these correspond to conditions in which multiple internal reflections within the system produce perfect constructive interference. In the framework of the PBGF formulation used here, the waveguide modes can be modeled by an evanescent wave excitation source from layer 0 of vanishingly small amplitude $E_{exi,p,0}$ such that the field, at some point z_{ref} within the waveguide layer, has unit amplitude. That is,

$$\lim_{k_{\rho,exi}\to k_s} \sum_{\sigma=\pm 1} G_p^{\sigma\sigma_{exi}}(k_{\rho,exi}, z_{ref}, Z_{exi})E_{exi,p,0} \to 1 \qquad (19)$$

This limit can be numerically approximated by setting $|\mathrm{k}_{\rho,exi} - \mathrm{k}_s|$ to some sufficiently small number, e.g., 10^{-6}.

At some particle origin $\mathbf{r}^i$ the exciting field can be represented by a regular VSWF expansion, per the usual plane wave formulas. The expansion coefficients are given by

$$f_{\mathbf{n},p}^i = \frac{1}{4\pi} e^{\mathrm{i}\mathrm{k}_{\rho,exi}\rho^i \cos(\phi_{exi}-\phi^i)} \sum_{\sigma=\pm 1} \Pi_{\mathbf{n},p}^\dagger(\sigma\mathrm{k}_{z,i},\phi_{inc}) G_p^{\sigma\sigma_{exi}}(\mathrm{k}_{\rho,exi},z^i,Z_{exi}) E_{exi,p,0} \quad (20)$$

2.2.5. Gaussian beam model

A Gaussian beam (GB) is characterized by a direction θ_{inc}, ϕ_{inc}, a focal point $\mathbf{r}^b$, and a (dimensionless) beam width at the focal point ω_b. It will be assumed that the GB originates from layer 0 and is propagating upwards ($\theta_{inc} < \pi/2$). The task at hand is to develop a workable formula for the regular VSWF expansion coefficients for the beam, centered about some arbitrary sphere origin $\mathbf{r}^i$ in the PB system. As has been done previously, the GB coefficients can be divided into direct and indirect parts,

$$f_{\mathbf{n},p}^i = \delta_{\ell(i)} f_{\mathbf{n},p,GB}(\mathbf{r}^i) + \widetilde{f}_{\mathbf{n},p,GB}(\mathbf{r}^i) \quad (21)$$

where the second, indirect part is due solely to reflection/transmission by the plane boundaries. The direct coefficients at $\mathbf{r}^i$ are related to those at the GB focal point by the regular VSWF translation operation [14, 15]:

$$f_{\mathbf{n},p,GB}(\mathbf{r}^i) = \sum_{\mathbf{l}} J_{\mathbf{nl}}(\mathrm{m}_0,\mathbf{r}^i-\mathbf{r}^b)\, f_{\mathbf{n},p,GB}^b \quad (22)$$

where J denotes the regular VSWF translation matrix, and the focal point coefficients $f_{\mathbf{n},p,GB}^b$ are functions solely of the beam width and propagation direction. The code uses the localized approximation for $f_{\mathbf{n},p,GB}^b$, which is appropriate for $\omega_b > 5$. The indirect coefficients are obtained from a modification of the regular VSWF translation operation to the PB system. The integral relation for the regular VSWF looks much like that for the outgoing function, Eq. (2), except the integration over the infinite plane is replaced by one over the sphere $\mathrm{k}_x^2 + \mathrm{k}_y^2 = \mathrm{m}^2$ and the result is divided by 2. In this respect, the plane wave spectrum of the regular VSWF at some position $z > 0$ contains only propagating waves, directed both upwards and downwards, whereas the outgoing VSWF spectrum at the same point would contain both propagating and evanescent waves that are directed only upwards. It is assumed that the direct part of the GB field can be described by a spectrum of upward–directed propagating waves (see, e.g., [14]), and accordingly the regular VSWF integral formula can be limited to only the upward–directed waves insofar as the expansion for the GB field is concerned. These waves will be reflected and transmitted by the plane boundaries, and the amplitude and phase of the waves, at some arbitrary point z, will be described by the indirect PBGF.

The indirect GB coefficients can therefore be obtained from an operation analogous to Eq. (22)

$$\widetilde{f}_{\mathbf{n},p,GB}(\mathbf{r}^i) = \sum_{\mathbf{l}} \mathrm{Rg}\,\widetilde{G}_{\mathbf{nl}}(\mathbf{r}^i,\mathbf{r}^0)\, f_{\mathbf{l},p,GB}(\mathbf{r}^0) \quad (23)$$

where $\mathrm{Rg}\,\widetilde{G}_{\mathbf{nl}}(\mathbf{r}^i,\mathbf{r}^0)$ is obtained from Eq. (10) (using the indirect PBGF), except divided by 2 and with an upper integration limit of m_0. The coefficients $f_{\mathbf{l},p,GB}(\mathbf{r}^{b'})$ are obtained

8

using Eq. (22), with $\mathbf{r}^{b'}$ having the same lateral position as $\mathbf{r}^b$ and a z position slightly below the first boundary (i.e., below 0); this translation is only necessary if the focal point $z^b > 0$.

2.2.6. Scattered field in the plane boundary system

The scattered field from sphere j, evaluated at some point $\mathbf{r}$ having local refractive index m, can be obtained from the MGF via

$$\mathbf{E}_{sca,p}^j(\mathbf{r}) = \sum_{\mathbf{n}} \sum_{\mathbf{l}} \mathbf{N}_{\mathbf{n}}^{(1)}(\mathsf{m}, \mathbf{r} - \mathbf{r}') G_{\mathbf{nl}}(\mathbf{r}', \mathbf{r}^j)\, a_{\mathbf{l},p}^j \tag{24}$$

where $a_{\mathbf{l},p}^j$ denote the scattering coefficients for sphere j with exciting polarization p, and $\mathbf{r}'$ is simply a secondary origin upon which the regular VSWF expansion is centered. For the free space case, convergence of the expansion requires $|\mathbf{r} - \mathbf{r}'| < |\mathbf{r}' - \mathbf{r}^j|$, and the convergence criteria become more complicated in the presence of plane boundaries. Such considerations are obviated by taking the limit of $\mathbf{r}' \to \mathbf{r}$, for which only the first TE degree of the regular VSWF survives. This leads to a general formula for the scattered field at an arbitrary point $\mathbf{r}$:

$$\mathbf{E}_{sca,p}^j(\mathbf{r}) = \sum_{j=1}^{N_s} \sum_{m=-1}^{1} \sum_{\mathbf{l}} \mathbf{P}_m G_{(1m1)\mathbf{l}}(\mathbf{r}', \mathbf{r}^j)\, a_{\mathbf{l},p}^j \tag{25}$$

with $\mathbf{P}_m$ denoting the cartesian vector

$$\mathbf{P}_{-1} = \frac{1}{\sqrt{6\pi}} \begin{pmatrix} 1 \\ -\mathsf{i} \\ 0 \end{pmatrix}, \quad \mathbf{P}_0 = \frac{1}{\sqrt{3\pi}} \begin{pmatrix} 0 \\ 0 \\ 1 \end{pmatrix}, \quad \mathbf{P}_1 = \frac{-1}{\sqrt{6\pi}} \begin{pmatrix} 1 \\ \mathsf{i} \\ 0 \end{pmatrix} \tag{26}$$

Numerical evaluation of the field in this exact manner is made difficult by the numerical integration requirements necessary to calculate the MGF at each particular point $\mathbf{r}$. It is, however, relatively easy to show, by use of the stationary phase approximation in Eq. (2), that the scattered field from the particles, evaluated at a distance $|z| >> R_C$ from the boundaries, reduces to an outgoing, hemispherical transverse wave [9]. The p-polarized component of the wave in layer 0, at a point $r, \theta_{sca}, \phi_{sca}$ on the hemisphere and resulting from a q-polarized exciting field, will be given by

$$E_{sca,pq}(r, \theta_{sca}, \phi_{sca}) = \frac{1}{r} e^{\mathsf{i}\mathsf{m}_0 r} A_{pq}^-(\mathsf{k}_{\rho,sca}, \phi_{sca}) \tag{27}$$

in which $A_{pq}^-(\mathsf{k}_{\rho,sca}, \phi_{sca})$ denotes the amplitude matrix for downward–propagating scattered waves:

$$A_{pq}^-(\mathsf{k}_{\rho,sca}, \phi_{sca}) = \sum_{j=1}^{N_S} \left[\frac{\mathsf{m}_0 \mathsf{k}_{z,0}}{\mathsf{m}_{\ell(j)}^2 \mathsf{k}_{z,j}} e^{-\mathsf{i}\mathsf{k}_{\rho,sca} \rho^j (\cos(\phi_{sca} - \phi^j))} \right.$$
$$\left. \times \sum_{\mathbf{n}} \sum_{\sigma'=\pm 1} \Pi_{\mathbf{n},p}(\sigma' \mathsf{k}_{z,j}, \phi_{sca})\, a_{\mathbf{n},q}^j G_p^{-1\sigma'}(\mathsf{k}_{\rho,sca}, Z_{-B}, z^j) \right] \tag{28}$$

9

with $a_{\mathbf{n},q}^{j}$ the scattered field expansion coefficients for particle j with excitation polarization q. The lateral wavenumber $\mathsf{k}_{\rho,sca} = \mathsf{m}_0 \sin \theta_{sca}$, and the normal wavenumbers $\mathsf{k}_{z,j}$ are obtained from $\mathsf{k}_{\rho,sca}$ via Eq. (4). Since layer 0 is lossless, changing the target position Z_{-B} will change only the phase of the amplitude matrix. Note that the amplitude matrix is defined relative to the plane parallel system: incident polarization state q is referenced with respect to the $\mathbf{k}_{exi} - \hat{z}$ plane, and scattered polarization state with respect to the $\mathbf{k}_{sca} - \hat{z}$. In this regard, the linear relationship between the incident and scattered Stokes vectors would be more appropriately referred to as a phase matrix as opposed to a scattering matrix [16]. The elements of the phase matrix are calculated from the amplitude matrix using the standard formulas [17, 16].

When the upper layer (layer $N_B + 1$) is lossless it is valid to define an analogous amplitude matrix for upwards–scattered waves, A^+; for this case the wavenumbers and refractive indices for layer 0 in Eq. (28) are replaced with those for the upper layer, the Green's function first direction superscript is made $+1$, and the function target point is evaluated at a reference position Z_{+B} above the uppermost particle. For a set lateral wavenumber $\mathsf{k}_{\rho,sca}$, $\sin \theta_{sca}$ will be different in the lower and upper layers when the refractive indices are different.

2.2.7. Cross sections and energy transfer

The presence of plane boundaries makes necessary an expanded definition of the cross sections associated with net EM energy transfer. Extinction by a particle – that being the removal of EM energy propagating in the direction of the exciting wave – can now occur in the two directions corresponding to reflection and transmission of the incident wave by the plane boundary system. Likewise, it will be useful to know the fraction of energy scattered into the front and back half spaces. Multiple plane boundaries also allow for the possibility of energy transfer via guided waves that are excited by scattering from the spheres.

A absorption cross section for particle i under $p-$polarized incidence, denoted as $C_{abs,i,p}$, can be derived by integration of the radial component of the Poynting vector $\mathbf{S}$ over the surface of the particle. The formula for $C_{abs,i,p}$ explicitly depends on the VSWF expansion coefficients for the exciting and scattered fields for particle i, and needs no alterations to account for the presence of plane boundaries or absorbing external media [18]. The total cross section by the entire set of particles is the sum of the individual particle cross sections:

$$C_{abs,p} = \sum_{i=1}^{N_S} C_{abs,i,p} \tag{29}$$

A total extinction cross section can be obtained by application of the extinction theorem to the exciting and scattered fields in layers 0 and N_B.

$$C_{f-ext,p} = C_{f-ext,p}^{+1} + C_{f-ext,p}^{-1} \tag{30}$$

$$C_{f-ext,p}^{\sigma} = -2\pi \mathrm{Re} \left[\sum_{q=1}^{2} \left(G_q^{\sigma\sigma_{exi}}(\mathsf{k}_{\rho,exi}, Z_{\sigma B}, Z_{exi}) \right)^* A_{qp}^{\sigma}(\mathsf{k}_{\rho,exi}, \phi_{exi}) \right] \tag{31}$$

The cross sections $C_{f-ext,p}^{-1}$ and $C_{f-ext,p}^{1}$ characterize the net removal of energy, due to the particles, from the reflected and transmitted exciting waves as measured by a collimated detector located in the far–field layers; $f - ext$ stands for 'far-field extinction'

10

and is needed as a different definition of extinction will be introduced below. The extinction cross sections are defined so that the total monochromatic extinction power is $I_0 C_{f-exp,p}/\mathrm{k}_0^2$, where I_0 is the exciting plane wave intensity. The transmission extinction is meaningful only for the case of a non–absorbing upper layer; for this condition the extinction will be independent of the reference position Z_{+B}. An absorbing upper medium, on the other hand, would result in an exponential decay of $C_{f-ext,p}^1$ with increasing Z_{+B}, and in this regard the 'far–field' transmission extinction should be taken as zero for this situation.

The total far–field scattering cross section can also be split into downward and upward parts, with each part obtained from a hemispherical integration of the scattered flux:

$$C_{f-sca,p} = C_{f-sca,p}^{+1} + C_{f-sca,p}^{-1} \tag{32}$$

$$C_{f-sca,p}^{\sigma} = \int_0^{2\pi} \int_0^1 \sum_{q=1}^2 \left| A_{qp}^{\sigma}(\sin\theta_{sca}, \phi_{sca}) \right|^2 d\cos\theta_{sca} d\phi_{sca} \tag{33}$$

For lossless systems consisting of two or more plane boundaries, scattered energy can be removed via guided slab waveguide modes. A measure of such effects can be obtained by returning to the equation for the particle scattering coefficients, Eq. (1). After some multiplication, rearranging, and application of translation matrix properties, one obtains a fundamental energy balance for the multiple sphere system:

$$C_{abs,p} = -\pi \operatorname{Re} \sum_{i=1}^{N_S} \sum_{\mathbf{n}} \left| \mathbf{a}_{\mathbf{n},p}^i \right|^2 \left(\frac{1}{\overline{a}_{\mathbf{n}}^i} + 1 \right) \tag{34}$$

$$= -\pi \sum_{i=1}^{N_S} \sum_{\mathbf{n}} \left[\left| \mathbf{a}_{\mathbf{n},p}^i \right|^2 + \operatorname{Re} \left[\mathbf{a}_{\mathbf{n},p}^{i*} \sum_{j=1}^{N_S} \sum_{\mathbf{l}} G_{\mathbf{nl}}(\mathbf{r}^i, \mathbf{r}^j) \mathbf{a}_{\mathbf{l},p}^j \right] - \operatorname{Re} \left[\mathbf{a}_{\mathbf{n},p}^{i*} f_{\mathbf{n},p}^i \right] \right]$$

$$= -C_{i-sca,p} - C_{d-sca,p} + C_{s-ext,p} \tag{35}$$

where $C_{i-sca,p}$, $C_{d-sca,p}$ and $C_{s-ext,p}$ are referred to as independent scattering, dependent scattering, and extinction cross sections at the sphere level. Each of these three terms corresponds to the result obtained by integration of a Poynting vector over the surface of sphere i and summed over i. For the independent scattering term the Poynting vector is formed solely from the outgoing scattered field from i, and for the dependent term the Poynting vector is formed from the superposition of the outgoing scattered field from i and the regular, multiply–scattered field due to the presence of the spheres. The extinction term in Eq. (35) has the Poynting vector formed from the superposition of the outgoing scattered field and regular exciting field at i, and for the case of lossless layers it can be shown that this cross section is equal to that obtained from Eq. (30) via the extinction theorem. The same equivalence, however, will not always occur between the scattering cross sections in Eq. (35) and that in Eq. (32). Specifically, a waveguide cross section can be defined via

$$C_{w-sca,p} = C_{i-sca,p} + C_{d-sca,p} - C_{f-sca,p} \tag{36}$$

and for lossless layers the overall energy balance appears as

$$C_{abs,p} + C_{f-sca,p} + C_{w-sca,p} = C_{s-ext,p} \tag{37}$$

11

Equation (37) states, simply, that the total energy removed from the exciting field by the spheres is distributed into absorption within the spheres, scattering into the far fields of layers 0 and N_B, and scattering that is trapped within a slab waveguide mode if/when such modes exist. As was mentioned in the previous section, waveguide modes can occur for systems of two or more plane boundaries, and are revealed by the existence of singular points in k_ρ for the PBGF. It can be shown (after several pages of formulas) that $C_{i-sca,p} + C_{d-sca,p}$ in Eq. (35) can be split into two integral terms, both involving a modified form of Eq. (10) for the MGF. The first term has the integration over k_ρ confined to propagating waves, and this part will correspond to the far–field scattering cross sections of Eq. (33). The integration for the second term has k_ρ limited to evanescent waves. This part will be zero except for the case when the PBGF has singular points, and the contribution due to the singular points can be obtained from the residue theorem evaluated at the singular points. That said, the more practical way to compute the waveguide cross sections is via the formulas in Eqs. (36), (35), and (33).

2.3. 2–D Periodic systems

2.3.1. 2–D periodic fundamentals

The system of N_S spheres is now taken to reside laterally within a rectangular, $W_x \times W_y$ unit cell, and this cell is repeated periodically in the x, y plane to $\pm\infty$ in both directions. The details of the plane boundaries and the exciting field remain the same.

The number of spheres in the system is now infinite, and, at least initially, Eq. (1) would appear to contain an infinite number of unknowns. It is relatively easy to show, however, that the sphere scattering coefficients in one unit cell, say located at position $(X_c, Y_c) = (c_x W_x, c_y W_y)$ with integer c_x, c_y, are related periodically to those in the central unit cell $(c_x, c_y) = (0, 0)$ by

$$a_{\mathbf{n}}^i(c_x, c_y) = e^{i(k_{x,exi}c_x W_x + k_{y,exi}c_y W_y)} a_{\mathbf{n}}^i(0,0) = e^{i\,\mathbf{k}_{\rho,exi}\cdot\mathbf{W}\cdot\mathbf{c}} a_{\mathbf{n}}^i(0,0) \qquad (38)$$

with $\mathbf{W} = W_x \hat{\mathbf{x}}\hat{\mathbf{x}} + W_y \hat{\mathbf{y}}\hat{\mathbf{y}}$ and $\mathbf{c} = c_x \hat{\mathbf{x}} + c_y \hat{\mathbf{y}}$. The 2–D periodic problem, therefore, has the same basic form as the finite problem:

$$a_{\mathbf{n}}^i = \overline{a}_{\mathbf{n}}^i \left(f_{\mathbf{n}}^i + \sum_{j=1}^{N_S} \sum_{\mathbf{l}}^{M_S^j} G_{\mathbf{nl}}^L(\mathbf{r}^i, \mathbf{r}^j) a_{\mathbf{l}}^j \right) \qquad (39)$$

The lattice MGF (LMGF) is formally defined by

$$G_{\mathbf{nl}}^L(\mathbf{r}, \mathbf{r}') = \sum_{\mathbf{c}} e^{i\,\mathbf{k}_{\rho,exi}\cdot\mathbf{W}\cdot\mathbf{c}} G_{\mathbf{nl}}(\mathbf{r}, \mathbf{r}' + \mathbf{W} \cdot \mathbf{c}) \qquad (40)$$

with $c_x, c_y = -\infty : \infty$.

The primary variables of the LMGF in Eq. (40) are the normal positions $z = \hat{\mathbf{z}} \cdot \mathbf{r}$ and $z' = \hat{\mathbf{z}} \cdot \mathbf{r}'$ and lateral displacement vector $\boldsymbol{\rho}_0 = \hat{\mathbf{x}}(x - x') + \hat{\mathbf{y}}(y - y')$. It is implicitly a function of the lateral exciting wavevector $\mathbf{k}_{\rho,exi}$, cell width $\mathbf{W}$ and the specifics of the plane boundary system. For all cases the lateral displacement can be shifted so that

$$G_{\mathbf{nl}}^L(\boldsymbol{\rho}_0, z, z') = e^{i\,\mathbf{k}_{\rho,exi}\cdot\mathbf{W}\cdot\mathbf{n}_p} G_{\mathbf{nl}}^L(\boldsymbol{\rho}, z, z') \qquad (41)$$

with

$$\boldsymbol{\rho} = \boldsymbol{\rho}_0 - \mathbf{n}_p \cdot W \tag{42}$$

$$n_{p,x} = \text{floor}\left(\frac{x_0 + W_x/2}{W_x}\right), \quad n_{p,y} = \text{floor}\left(\frac{y_0 + W_y/2}{W_y}\right) \tag{43}$$

As was done in Eq. (12), the LMGF can be split into regular and free–space parts:

$$G^L_{\mathbf{nl}}(\boldsymbol{\rho}, z, z') = \widetilde{G}^L_{\mathbf{nl}}(\boldsymbol{\rho}, z, z') + \delta_{\ell-\ell'} L_{\mathbf{nl}}(\boldsymbol{\rho}, z - z') \tag{44}$$

with ℓ, ℓ' denoting the layers containing z and z'; the free–space part appears only when z and z' are in the same layer and the regular part occurs only when plane boundaries are present.

2.3.2. Free space case

The free space LMGF, L, can be obtained from the lattice sum of the scalar spherical wave function (SSWF), which is defined by

$$u_{vw}(\mathsf{m}, \mathbf{r}) = \sum_{\mathbf{c}} \psi^{(3)}_{vw}(\mathsf{m}, \mathbf{r} - \mathbf{W} \cdot \mathbf{c}) e^{\mathrm{i}\,\mathbf{k}_{\rho,exi} \cdot \mathbf{W} \cdot \mathbf{c}} \tag{45}$$

This formula is not used in actual numerical practice as the series is poorly converging when $\mathrm{Im}\,\mathsf{m}$ is zero or small. The central unit cell $\mathbf{c} = (0,0)$ contribution may or may not be included in this sum; this part must be omitted when $|\mathbf{r}| = 0$ as the sum would otherwise be singular. The matrix elements of L are

$$L_{mnp\,klq} = -(-1)^m \mathrm{i}^{n-l} \sqrt{4\pi(2n+1)(2l+1)} \sum_{w=w_1,2}^{w_2} \frac{\mathrm{i}^w}{\sqrt{2w+1}} C^w_{-1n\,1l} C^w_{-mn\,kl} u_{k-m\,w} \tag{46}$$

$$w_1 = |n - l| + |p - q|, \quad w_2 = n + l - |p - q| \tag{47}$$

with $C^w_{mn\,kl} = C(n, m; l, k; w, m + k)$ denoting the Clebsch-Gordon coefficient.

Numerical methods for u are based on the integral relation for the scalar wave function:

$$\psi^{(3)}_{mn}(\mathsf{m}, \mathbf{r}) = h_n(\mathsf{m}r) Y_{mn}(\hat{\mathbf{r}}) = -\frac{(-\mathrm{i})^n}{2\pi} \int_{-\infty}^{\infty} d\mathsf{k}_a \int_{-\infty}^{\infty} d\mathsf{k}_b \, Y_{mn}(\mathbf{k}) \, e^{\mathrm{i}\,\mathsf{m}\mathbf{k}\cdot\mathbf{r}} \frac{1}{\mathsf{m}^2\mathsf{k}_c} \tag{48}$$

in which the subscripts (a, b) refer to unit orthogonal vectors in the plane over which the wavevector $\mathbf{k}$ is integrated. The direction normal to the plane is $\hat{\mathbf{e}}_c = \hat{\mathbf{e}}_a \times \hat{\mathbf{e}}_b$, and

$$\mathbf{k} = \frac{1}{\mathsf{m}} (\mathsf{k}_a \hat{\mathbf{e}}_a + \mathsf{k}_b \hat{\mathbf{e}}_b + \mathsf{k}_c \hat{\mathbf{e}}_c) \tag{49}$$

$$\mathsf{k}_c = \left(\mathsf{m}^2 - \mathsf{k}_a^2 - \mathsf{k}_b^2\right)^{1/2} \text{sign}\left(\mathbf{r} \cdot \hat{\mathbf{e}}_c\right) \tag{50}$$

Equation (48) has a finite value only for $|\mathbf{r} \cdot \hat{\mathbf{e}}_c| > 0$. The component k_c will become imaginary whenever $\mathsf{k}_a^2 + \mathsf{k}_b^2 > \mathsf{m}^2$, and the choice of the sign of k_c insures a decaying exponential in Eq. (48) and thus convergence of the integration in the $a-b$ plane. Observe that the argument of the spherical harmonic in Eq. (48) is defined relative to the $\hat{\mathbf{x}}$, $\hat{\mathbf{y}}$, $\hat{\mathbf{z}}$ coordinate system and not $\hat{\mathbf{e}}_a$, $\hat{\mathbf{e}}_b$, $\hat{\mathbf{e}}_c$, i.e., the argument of the Legendre function is $\hat{\mathbf{z}} \cdot \mathbf{k}$.

The code uses two numerical methods for u, depending on the values of z and $\mathbf{W}$. When $|z|$ is relatively large, specifically $|z| > W_{min}/2$, the integration coordinates $a = x$, $b = y$ are chosen. The summation over lattice sites in the $x - y$ plane can be performed analytically by use of Poisson's summation formula, and leads to

$$u_{vw} = \frac{2\pi(-\mathrm{i})^w}{W_x W_y \mathsf{m}^2} \sum_{\mathbf{s}} \frac{1}{\mathrm{k}_z^{\mathbf{s}}} e^{\mathrm{i}(\mathbf{k}_\rho^{\mathbf{s}} \cdot \boldsymbol{\rho} + \mathsf{m} \mathrm{k}_z^{\mathbf{s}} z)} Y_{vw}(\mathrm{k}_z^{\mathbf{s}}, \alpha^{\mathbf{s}}) \tag{51}$$

$$\mathbf{k}_\rho^{\mathbf{s}} = 2\pi \mathbf{s} \cdot \left(\frac{1}{\mathbf{W}}\right)^{-1} + \mathbf{k}_{\rho,exi}, \quad \mathrm{k}_z^{\mathbf{s}} = \mathrm{sign}\, z \sqrt{1 - |\mathbf{k}_\rho^{\mathbf{s}}|^2/\mathsf{m}^2}, \quad \alpha^{\mathbf{s}} = \tan^{-1}\left(\frac{\mathrm{k}_y^{\mathbf{s}}}{\mathrm{k}_x^{\mathbf{s}}}\right) \tag{52}$$

with $\mathbf{s} = s_x \hat{\mathbf{x}} + s_y \hat{\mathbf{y}}$. The sum runs through positive and negative integer values of s_x, s_y of increasing magnitude until convergence. This formula includes the contribution from the source in the central unit cell.

The formula in Eq. (51) is valid so long as $|z| \neq 0$, yet convergence becomes increasingly slow as $|z|$ gets small. There are a multitude of reported methods for efficiently and accurately evaluating the SSWF lattice sum when the evaluation point is in or near the plane of the lattice; the reader is referred to [19] for a comprehensive review. In the 2-D periodic free space scattering problem examined by [4], the lattice sums are numerically evaluated using the method originally developed by Ewald [20]. The Ewald method requires a number of special functions with complex argument, such as the incomplete Gamma function, and the author must also admit that he has never quite figured out how the Ewald method was derived nor how it works. Rather, for $|z| \leq W_{min}/2$, the code uses a procedure suggested (I believe) in [19] which omits the source at $\mathbf{c} = (0,0)$ in Eq. (45). It turns out that to exploit this procedure, mathematical and numerical advantages are obtained by orienting the lattice in the $y - z$ plane, so that $\mathbf{c} = c_y \hat{\mathbf{y}} + c_z \hat{\mathbf{z}}$ in Eq. (45); a subsequent rotation operation on the sum can return the lattice to the original $x - y$ convention.

The $y - z$ lattice sum can be broken up into four parts: a pair of 1-D sums with $c_z = 1 : \infty$ and $-\infty : -1$, each having $c_y = 0$, and a pair of 2-D sums from $c_y = 1 : \infty$ and $-\infty : -1$, each having $c_z = -\infty : \infty$. The 1-D case uses $c = z$ in Eq. (48) and converts the integration domain to cylindrical coordinates: $d\mathrm{k}_x d\mathrm{k}_y = \mathrm{k}_\rho d\mathrm{k}_\rho d\alpha$. The integration over α is performed analytically to obtain a Hankel-transform type formula. The summation over c_z is also performed analytically, and the remaining integration over k_ρ is performed by deforming the integration path onto a complex contour that smoothes and accelerates the convergence of the integrand. The 2-D case uses $c = y$ in Eq. (48). This allows use of Poisson's formula on the summation over c_z, which replaces the integration over the z direction with a summation over reciprocal lattice in s_z. The summations over y can be performed analytically, and a steepest descent contour is again used to smooth out the remaining numerical integration.

The rotation operation that transforms the $y - z$ lattice sum into the $x - y$ lattice sum is

$$u_{mn}(x, y, z, \mathrm{k}_{x,exi}, \mathrm{k}_{y,exi}, W_x, W_y)$$
$$= (-1)^n \sum_{k=-n}^{n} \mathcal{D}_{mk}^{(n)}(0)\, u'_{kn}(z, -y, x, -\mathrm{k}_{y,exi}, \mathrm{k}_{x,exi}, W_y, W_x) \tag{53}$$

14

with $\mathcal{D}(\cos\theta)$ being the generalized spherical function. The $y - z$ lattice sum, u', is formed from the 1–D and 2–D parts,

$$u'_{mn}(x', y', z', \mathrm{k}'_{y',exi}, \mathrm{k}'_{z',exi}, W'_{y'}, W'_{z'})$$
$$= (-\mathrm{i})^{n-m+1} e^{im\phi'} Q^{(1)}_{mn}(\rho', z', \mathrm{k}'_{z',exi}, W'_{z'})$$
$$- \frac{(-\mathrm{i})^n}{\mathsf{m}W'_{z'}} \sum_{s=-\infty}^{\infty} Y_{mn}(\mathrm{k}^s_\rho/\mathsf{m}, 0) e^{\mathrm{i}\mathrm{k}^s_\rho z'} Q^{(2)}_m(\mathrm{k}^s_\rho, x', y', \mathrm{k}'_{y',exi}, W'_{y'}) \quad (54)$$

where

$$\rho' = \sqrt{x'^2 + y'^2}, \quad \phi' = \tan^{-1}\left(\frac{y'}{x'}\right), \quad \mathrm{k}^s_\rho = \mathrm{k}'_{z',exi} + \frac{2\pi s}{W'_{z'}} \quad (55)$$

with the sum over s typically converging in ceiling $(W'_{z'}/2\pi)$ terms. The functions $Q^{(1)}_{mn}$ and $Q^{(2)}_m$ are given by the integral relations

$$Q^{(1)}_{mn}(\rho', z', \mathrm{k}'_{z',exi}, W'_{z'}) = \int_0^\infty Y_{mn}(u, 0) J_m(\mathsf{m}\rho'v) \left(f_1 + (-1)^{m+n} f_2\right) dt \quad (56)$$

$$u = 1 + \mathrm{i}t, \quad v = \sqrt{1 - u^2} \quad (57)$$

$$f_1 = e^{imu(W'_{z'}+z')} \left(e^{\mathrm{i}\mathrm{k}'_{z',exi}W'_{z'}} - e^{imuW'_{z'}}\right)^{-1} \quad (58)$$

$$f_2 = e^{imu(W'_{z'}-z')} \left(e^{-\mathrm{i}\mathrm{k}'_{z',exi}W'_{z'}} - e^{imuW'_{z'}}\right)^{-1} \quad (59)$$

and

$$Q^{(2)}_m(\mathrm{k}^s_\rho, x', y', \mathrm{k}'_{y',exi}, W'_{y'}) = \int_{-\infty}^\infty \left(f_1 \left(\frac{u - \mathrm{i}v}{w}\right)^m + f_2 \left(\frac{u + \mathrm{i}v}{w}\right)^m\right) e^{imux'} \frac{1}{v} \frac{du}{dt} dt \quad (60)$$

$$w = \sqrt{1 - (\mathrm{k}^s_\rho/\mathsf{m})^2}, \quad u = t\sqrt{t^2 - 2iw}, \quad v = \sqrt{w^2 - u^2} \quad (61)$$

$$f_1 = e^{imv(W'_{y'}-y')} \left(e^{im\,vW'_{y'}} - e^{-\mathrm{i}\mathrm{k}'_{y',exi}W'_{y'}}\right)^{-1} \quad (62)$$

$$f_2 = e^{imv(W'_{y'}+y)} \left(e^{imvW'_{y'}} - e^{\mathrm{i}\mathrm{k}'_{y',exi}W'_{y'}}\right)^{-1} \quad (63)$$

Numerical integration of Eqs. (56) and (60) is performed using the same Gauss–Kronod scheme used for Eq. (10). The integrals are broken into finite segments of length $\Delta t \sim 1/W$ and the GK algorithm is applied to each segment.

2.3.3. Plane boundary system contribution

The plane boundary contribution is obtained from a 2-D reciprocal space summation:

$$\widetilde{G}^L_{\mathbf{nl}}(\boldsymbol{\rho}, z, z') = \frac{8\pi^2}{W_x W_y} \sum_{\mathbf{s}} K^{\mathbf{s}}_{\mathbf{nl}}(\boldsymbol{\rho}, z, z') \quad (64)$$

15

with

$$K_{mnpklq}^{\mathbf{s}}(\boldsymbol{\rho}, z, z') = e^{i(k-m)\alpha^{\mathbf{s}}} \, e^{i\mathbf{k}_\rho^{\mathbf{s}}\cdot\boldsymbol{\rho}} \, \frac{1}{\mathrm{k}_{z,\ell'}\mathsf{m}_{\ell'}^2}$$

$$\sum_{\sigma=\pm 1}\sum_{\sigma'=\pm 1}\sum_{t=1}^{2}\Big(\sigma^{m+n+p}\sigma'^{k+l+q}(\sigma\sigma')^{t-1}$$

$$\times\, \Pi_{mnp,t}^{\dagger}(\mathrm{k}_{z,\ell}^{\mathbf{s}},0)\widetilde{G}_t^{\sigma\sigma'}(\mathrm{k}_\rho^{\mathbf{s}}, z, z')\Pi_{klq,t}(\mathrm{k}_{z,\ell'}^{\mathbf{s}},0)\Big) \quad (65)$$

$$\mathbf{k}_\rho^{\mathbf{s}} = 2\pi\mathbf{s}\cdot(\mathbf{W})^{-1} + \mathbf{k}_{\rho,exi}, \quad \mathrm{k}_{z,\ell} = \sqrt{1 - |\mathbf{k}_\rho|^2/\mathsf{m}_\ell^2} \quad (66)$$

Note that the formula uses the regular form of the PBGF, which omits the direct interaction between z and z' when both are in the same layer; this contribution is included in the free space part of Eq. (44).

2.3.4. Scattered field

The scattered field from the periodic lattice appears as a discrete set of plane waves, with lateral wavevectors given by the reciprocal lattice vector $\mathbf{k}_\rho^{\mathbf{s}}$ defined in Eq. (66) [21]. The amplitude matrix for periodic system is the same as Eq. (28), except now multiplied by $8\pi/(W_x W_y)$. Given a (propagating) exciting plane wave of incidence θ_{inc}, ϕ_{inc} and polarization p, the reflectance of the lattice is

$$R_p(\theta_{inc}, \phi_{inc}) = \frac{1}{\mathsf{m}_0 \cos\theta_{inc}}\sum_{\mathbf{s}}\sum_{q=1}^{2}\mathrm{k}_{z,0}^{\mathbf{s}}\left|A_{qp}^{L,-}(\mathbf{k}_\rho^{\mathbf{s}})\right|^2 \quad (67)$$

The sum over reciprocal lattice index includes only those modes for which $\mathrm{k}_{z,0}^{\mathbf{s}}$ is real.

2.4. Code compilation and execution

The MSTM fortran–90 code is available for download at [22]. The gfortran compiler and MS Windows OS were the primary platforms used to develop and test the code. Options are available for generating serial code, and parallel code using the message passing interface (MPI) convention; details of the compilation procedure are provided in the documentation accompanying the code.

The code does not employ a fancy user interface. Execution occurs via a command–line invocation of the code with an associated input file, i.e.,

```
mstm.exe mstm.inp
```

where `mstm.exe` and `mstm.inp` refer to the executable and input file names. The details of the sphere/plane boundary system to be analyzed, the calculation options and parameters used, and the type and destination of the output results, are all contained in the input file. The code website contains several example input files with associated calculation output files, including all of the calculations used in this paper. Found also at the website are Mathematica notebook files used for post–processing of calculation results.

3. Example results

A series of example calculation results are now presented, the objective of which primarily is to demonstrate the veracity of the formulation and code.
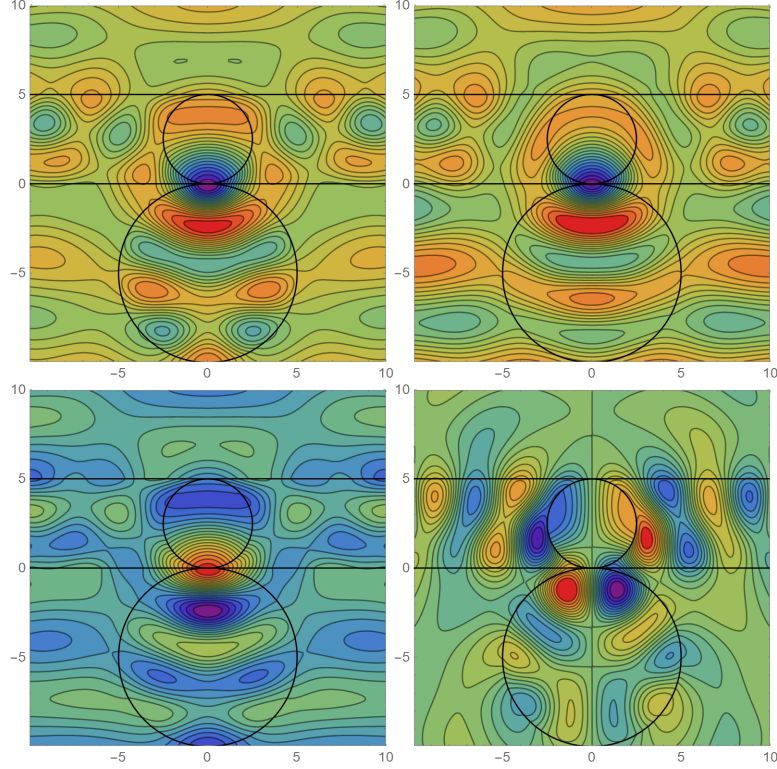
16

Figure 1: Internal fields in the $x - z$ plane for a sphere–thin film system. Clockwise from top left: $H_{y,1}$, $E_{y,2}$, $H_{z,2}$, $H_{x,2}$, with second subscript 1,2 denoting incident polarization parallel or perpendicular to plane.

3.1. Spheres on and/or in thin films

The code includes features to efficiently calculate the electric and magnetic complex field amplitudes on a 1-D, 2-D, or 3-D grid of points. An example of such calculation results is presented in Fig. (1), which shows contour plots of dimensionless electric and magnetic field amplitudes within a sphere/plane boundary system. The system consists of a dielectric film ($H_1 = 5$, $\mathsf{m}_1 = 1.6$) in air, with a dielectric sphere ($a = 5$, $\mathsf{m} = 1.6$) externally on the bottom surface and a bubble ($a = 2.5$, $\mathsf{m} = 1$) centered in the film. The system is excited by a normally–incident plane wave, polarized in either the x or y direction, and the field lines are shown in the $x - z$ plane. The four field components shown were chosen as they, theoretically, should maintain continuity across the spherical and plane boundaries; this continuity is clearly evident in the plots. Calculation of the solution and the 4×10^4 points used in the figures took less than a minute on an HP Z820 workstation running on 8 cores.

The spheres in Fig. (1) excite waveguide modes within the film, which are revealed by a non–zero waveguide scattering cross section C_{w-sca}. As the waveguide modes, in this situation, result from the formation of evanescent fields between the sphere and plane boundaries, the cross section C_{w-sca} is exquisitely sensitive to the distance between
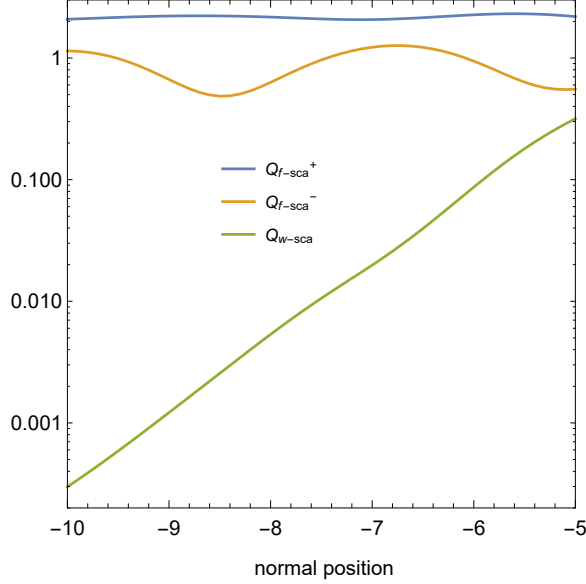
17

Figure 2: Scattering efficiencies vs. sphere position, for a sphere–thin film system.

these boundaries. This is demonstrated in Fig. (2), which shows the up and down farfield scattering efficiency and the waveguide efficiency, as a function of sphere z position, for a single sphere ($a = 5$, $\mathsf{m} = 1.6$) external to a film ($H_1 = 5$, $\mathsf{m}_1 = 1.6$). Efficiencies are defined as cross sections divided by πa^2, and the case of $z = -5$ corresponds to the sphere in contact with the lower surface of the film. As would be expected from an evanescent field effect, the waveguide efficiency is seen to drop off exponentially with distance of the sphere from the surface. Note that C^-_{f-sca} shows significant oscillatory behavior with a period $\sim \pi$; this suggests an effect of interference between the backscattered field from the sphere and the forward–scattered field that is reflected from the plane boundaries.

An demonstration of field patterns resulting from Gaussian beam excitation of a plane boundary system, either free of spheres or with spheres, is shown in Fig. (3). The required continuity of the field lines at the spherical and plane boundaries is again clearly evident.

3.2. Periodic systems

The sphere/plane boundary system used for Fig. (1) is now made periodic, using a square unit cell with $W_x = W_y = 10$; this results in the lower, $a = 5$ spheres coming into point contact with their periodic neighbors. Contour plots of the field distributions are shown in Fig. (4) for normal incidence. The plots demonstrate the required symmetry conditions along the left and right cell boundaries: under normal incidence conditions, the contour lines must intersect these boundaries at right angles.

An additional test of the periodic formulation is presented in Fig. (5). Shown is reflectance from a square periodic array of spheres, with $a = 2$, $\mathsf{m} = 1.6$, and $W = 4$, that are in contact with the exposed side of a $H = 4$, $\mathsf{m} = 1.6$ substrate, as a function of incident angle. Results are calculated using the present MSTM code and the plane
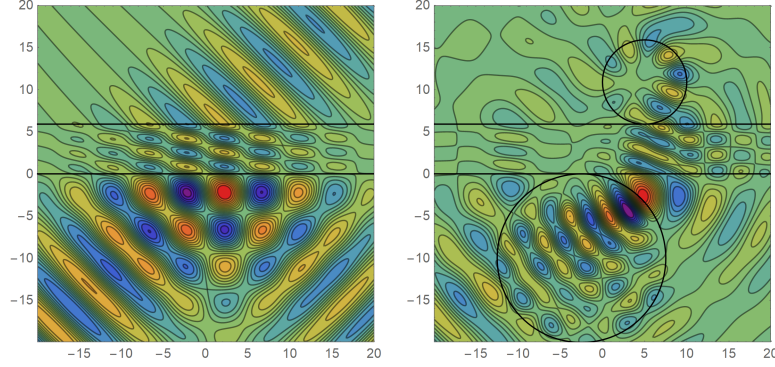
18

Figure 3: Electric field $E_{y,2}$ in the $x - z$ plane for a Gaussian beam excitation. Beam width $\omega_b = 20$, focal point $= (0,0,0)$. Slab $H = 5.9$, $\mathsf{m} = 2$. Left shows interaction of GB with PB system, right includes effects of two spheres, each having $\mathsf{m} = 1.6$.

wave plane parallel (PWPP) code of [23]. The two lines for each model correspond to incident polarization parallel and perpendicular to the incident–normal plane. The PWPP formulation is based on a 2–D Fourier–transformed volume integral solution. It is similar to a discrete dipole approximation in that it uses a volume–discretized representation of the scatterer, yet it is also distinct in that it automatically embeds the 2–D periodic character of the fields into the solution. Suffice to say that the PWPP mathematical model is distinctly different from the superposition solution used in MSTM, and the fact that both produce such good agreement in Fig. (5) suggests that both are valid results. Although not shown here, the current MSTM code has reproduced the silicon sphere lattice reflection results given in [3, 6].

4. Acknowledgements

References

[1] D. W. Mackowski, M. I. Mishchenko, A multiple sphere T-matrix Fortran code for use on parallel computer clusters, "J. Quant. Spectrosc. Radiat. Transfer" 112 (2011) 2182–2192.

[2] D. Mackowski, A general superposition solution for electromagnetic scattering by multiple spherical domains of optically active media, "J. Quant. Spectrosc. Radiat. Transfer" 133 (2014) 264 – 270.

[3] N. Stefanou, A. Modinos, Scattering of light from a two-dimensional array of spherical particles on a substrate, Journal of Physics: Condensed Matter 3 (41) (1991) 8135.

[4] D. Theobald, D. Beutel, L. Borgmann, H. Mescher, G. Gomard, C. Rockstuhl, U. Lemmer, Simulation of light scattering in large, disordered nanostructures using a periodic t-matrix method, J. Quant. Spectrosc. Radiat. Transfer 272 (2021) 107802. doi:https://doi.org/10.1016/j.jqsrt.2021.107802.
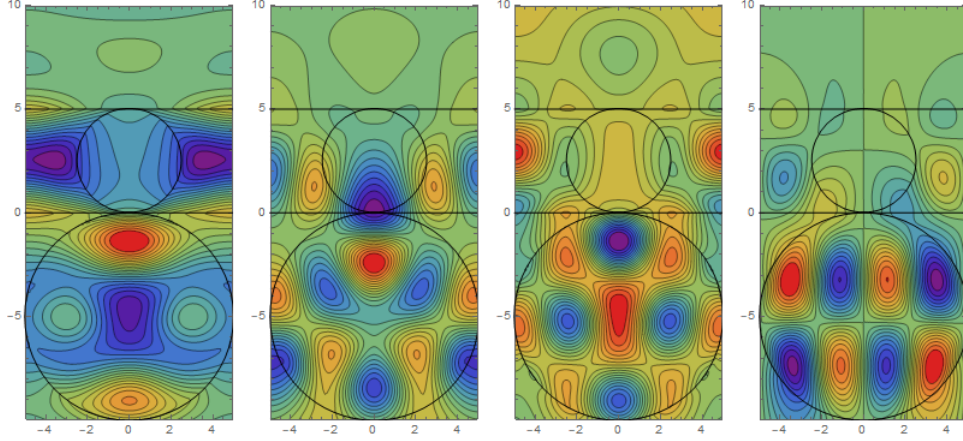URL https://www.sciencedirect.com/science/article/pii/S0022407321002958

Figure 4: Internal fields in the $x-z$ plane for a 2-D periodic sphere–thin film system. Cell width $W = 10$. Left to right $H_{y,1}$, $E_{y,2}$, $H_{z,2}$, $H_{x,2}$, with second subscript 1,2 denoting incident polarization parallel or perpendicular to plane.

[5] C. L. Holloway, E. F. Kuester, J. A. Gordon, J. O'Hara, J. Booth, D. R. Smith, An overview of the theory and applications of metasurfaces: The two-dimensional equivalents of metamaterials, IEEE Antennas and Propagation Magazine 54 (2) (2012) 10–35. doi:10.1109/MAP.2012.6230714.

[6] D. R. Abujetas, J. Olmos-Trigo, J. J. Sáenz, J. A. Sánchez-Gil, Coupled electric and magnetic dipole formulation for planar arrays of particles: Resonances and bound states in the continuum for all-dielectric metasurfaces, Phys. Rev. B 102 (2020) 125411. doi:10.1103/PhysRevB.102.125411. URL https://link.aps.org/doi/10.1103/PhysRevB.102.125411

[7] N. Razmjooei, Y. H. Ko, F. A. Simlan, R. Magnusson, Resonant reflection by microsphere arrays with ar-quenched mie scattering, Optics Express 29 (12) (2021) 19183–19192.

[8] P. A. Bobbert, J. Vlieger, Light scattering by a sphere on a substrate, Physica 137A (1986) 209–242.

[9] T. Wriedt, A. Doicu, Light scattering from a particle on or near a surface, Opt. Comm. 152 (1998) 376–384.

[10] D. W. Mackowski, Exact solution for the scattering and absorption properties of sphere clusters on a plane surface, J. Quant. Spectrosc. Radiat. Transfer 109 (2007) 770–788.

[11] D. W. Mackowski, A generalization of image theory to predict the interaction of multipole fields with plane surfaces, J. Quant. Spectrosc. Radiat. Transfer 111 (5) (2010) 802 – 809. doi:DOI: 10.1016/j.jqsrt.2009.11.016.
URL http://www.sciencedirect.com/science/article/B6TVR-4XSJVXC-2/2/9d8ff1f7079a704b0025c2ee0e09cb32

[12] A. Egel, S. W. Kettlitz, U. Lemmer, Efficient evaluation of sommerfeld integrals for the optical simulation of many scattering particles in planarly layered media, JOSA A 33 (4) (2016) 698–706.

[13] T. J. Cui, W. C. Chew, Fast evaluation of sommerfeld integrals for em scattering and radiation by three-dimensional buried objects, IEEE Trans. Geoscience Remote Sensing 37 (1999) 887–900.

[14] A. Doicu, T. Wriedt, Computation of the beam–shape coefficients in the generalized Lorenz–Mie theory by using the translational addition theorem for spherical vector wave functions, Appl. Opt. 13 (1997) 2971–2978.

[15] D. W. Mackowski, M. I. Mishchenko, Direct simulation of multiple scattering by discrete random media illuminated by Gaussian beams, Phys. Rev. A 83 (1) (2011) 013804–+. doi:10.1103/PhysRevA.83.013804.

[16] J. W. Hovenier, C. V. van der Mee, H. Domke, Transfer of polarized light in planetary atmospheres: basic concepts and practical methods, Vol. 318, Springer Science & Business Media, 2014.

[17] C. F. Bohren, D. R. Huffman, Absorption and Scattering of Light by Small Particles, Wiley, 1983.

[18] D. Mackowski, M. Mishchenko, Direct simulation of extinction in a slab of spherical particles, "J. Quant. Spectrosc. Radiat. Transfer" 123 (2013) 103 – 112.
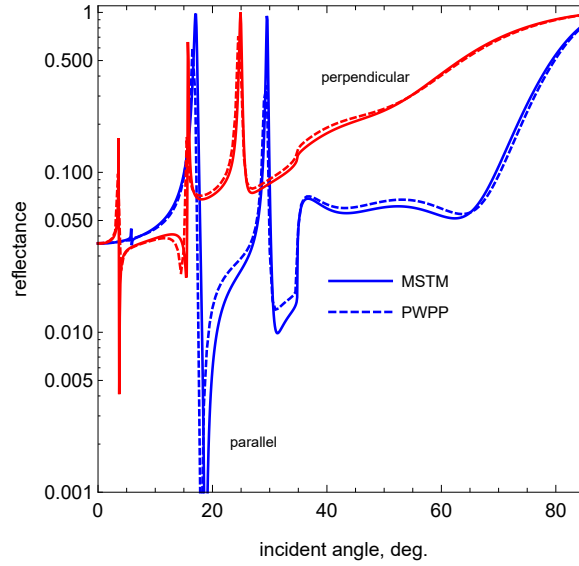
Figure 5: Reflectance from a square periodic array of spheres on a substrate. Sphere properties $a = 2$, $\mathsf{m} = 1.6$, lattice width $W = 4$, substrate properties $H = 4$, $\mathsf{m} = 1.6$.

URL `http://www.sciencedirect.com/science/article/pii/S0022407313000629`

[19] C. M. Linton, Lattice sums for the helmholtz equation, SIAM review 52 (4) (2010) 630–674.

[20] P. Ewald, Die berechnung optischer und elektrostatischer gitterpotentiale, Annalen der Physik 369 (3) (1921) 253–287.

[21] D. W. Mackowski, Van de Hulst Essay: The dda, the rte, and the computation of scattering by plane parallel layers of particles, J. Quant. Spectrosc. Radiat. Transfer 189 (2017) 43–59.

[22] Multiple–sphere codes are available at www.eng.auburn.edu/users/dmckwski/scatcodes.

[23] D. W. Mackowski, B. Ramezanpour, A plane wave model for direct simulation of reflection and transmission by discretely inhomogeneous plane parallel media, J. Quant. Spectrosc. Radiat. Transfer 213 (2018) 95–106.

Appendix

The Fresnel coefficients appearing in Eq. (13) are given by

$$T_1^{1\,1,n}(\mathrm{k}_\rho) = \frac{2\mathrm{m}_{n-1}\mathrm{k}_{z,n-1}}{\mathrm{m}_{n-1}\mathrm{k}_{z,n} + \mathrm{m}_n\mathrm{k}_{z,n-1}} \tag{68}$$

$$T_1^{1\,-1,n}(\mathrm{k}_\rho) = -T_1^{-1\,1,n}(\mathrm{k}_\rho) = \frac{\mathrm{m}_{n-1}\mathrm{k}_{z,n} - \mathrm{m}_n\mathrm{k}_{z,n-1}}{\mathrm{m}_{n-1}\mathrm{k}_{z,n} + \mathrm{m}_n\mathrm{k}_{z,n-1}} \tag{69}$$

$$T_1^{-1\,-1,n}(\mathrm{k}_\rho) = \frac{2\mathrm{m}_n\mathrm{k}_{z,n}}{\mathrm{m}_{n-1}\mathrm{k}_{z,n} + \mathrm{m}_n\mathrm{k}_{z,n-1}} \tag{70}$$

$$T_2^{1\,1,n}(\mathrm{k}_\rho) = \frac{2\mathrm{m}_{n-1}\mathrm{k}_{z,n-1}}{\mathrm{m}_{n-1}\mathrm{k}_{z,n-1} + \mathrm{m}_n\mathrm{k}_{z,n}} \tag{71}$$

$$T_2^{1\,-1,n}(\mathrm{k}_\rho) = -T_2^{-1\,1,n}(\mathrm{k}_\rho) = -\frac{\mathrm{m}_{n-1}\mathrm{k}_{z,n-1} - \mathrm{m}_n\mathrm{k}_{z,n}}{\mathrm{m}_{n-1}\mathrm{k}_{z,n-1} + \mathrm{m}_n\mathrm{k}_{z,n}} \tag{72}$$

$$T_2^{-1\,-1,n}(\mathrm{k}_\rho) = \frac{2\mathrm{m}_n\mathrm{k}_{z,n}}{\mathrm{m}_{n-1}\mathrm{k}_{z,n-1} + \mathrm{m}_n\mathrm{k}_{z,n}} \tag{73}$$

These formulas are equivalent to the Fresnel relations, i.e., $T_p^{-1\,1,n}$ and $T_p^{1\,1,n}$ are the Fresnel reflectance and transmittance for a wave incident on boundary n from below.